Simulating Melting in 2D Seismic Fault Gouge

G. Mollon, J. Aubry, A. Schubnel

JGR Solid Earth

RESEARCH ARTICLE
10.1029/2020JB021485

Simulating Melting in 2D Seismic Fault Gouge

Guilhem Mollon[1,2], **Jérôme Aubry**[2], **and Alexandre Schubnel**[2]

[1]Université de Lyon, LaMCoS, INSA-Lyon, CNRS UMR5259, Lyon, France, [2]Laboratoire de Géologie, École Normale Supérieure/CNRS UMR 8538, PSL Research University, Paris, France

Key Points:

- Simulations confirm that fault gouges naturally tend to localize shearing in a narrow area, corresponding to a few tens of grain diameter
- Molten grains in the fault gouge lead to a reduction in friction, which follows a sigmoid-like weakening phenomenology
- Melt presence leads to a more intense localization of the shearing, leading to a positive feedback to its own generation

Correspondence to:
G. Mollon,
guilhem.mollon@insa-lyon.fr

Citation:
Mollon, G., Aubry, J., & Schubnel, A. (2021). Simulating melting in 2D seismic fault gouge. *Journal of Geophysical Research: Solid Earth*, *126*, e2020JB021485. https://doi.org/10.1029/2020JB021485

Received 4 DEC 2020
Accepted 4 MAY 2021

Abstract During an earthquake, fault slip weakening is often explained by frictional heating phenomena, generally promoting melt production on the fault surface. Here, we investigate the influence of melt production at the scale of the grains composing a fault gouge. We use a modern version of Discrete Element Modeling able to deal with realistic grain shapes in 2D, and couple it with a Multibody Meshfree Approach able to provide a satisfactory proxy for the mechanical behavior of molten grains. Frictional sliding of solid grains and viscous shearing of molten grains are monitored during simulations. Our results confirm the natural tendency of granular gouge to localize deformation in a thin layer, and thus to trigger local melt production. We also show that the appearance of melt is likely to enhance this localization, and might create a positive feedback to its own production. We propose guidelines for the future writing of a friction model including melting, inspired by these simulation results.

1. Introduction

Fault weakening is a major phenomenon driving the dynamics of large earthquakes because the evolution of fault friction during slip controls dynamic stress drop and heat creation (Di Toro et al., 2006; Rice, 2006). As pointed out in Mair and Marone (2000), simple granular behaviors in the fault gouge cannot explain this phenomenon. Meanwhile, a large number of physical phenomena can promote fault weakening, including thermal pressurization (Wibberley & Shimamoto, 2005), thermal decomposition (Han et al., 2007; Sulem et al., 2009), nanopowder (Han et al., 2010), gel lubrications (Goldsby & Tullis, 2002; Di Toro et al., 2004), superplasticity in coseismic ultramylonites (Pozzi et al., 2019), flash heating of asperities and fault gouge melting. Recent high-velocity experiments documented these last two phenomena and confirmed that flash heating at contacting asperities occurs rapidly and leads to localized patches of molten rock which can eventually merge and pervasively lubricate the fault (Hirose & Shimamoto, 2005; Goldsby & Tullis, 2011). According to this model, the very first stage of frictional sliding can be computed by a linear mixing law between undeformed (i.e., intact) and flash-heated asperities (Rice, 2006). In this model, the balance between these asperity populations is controlled by the ratio of the sliding velocity to a certain characteristic weakening velocity. This model was further used in a dynamic model, in combination with rate-and-state friction (RSF) laws (Bizzari, 2009). It also showed good agreement with the experimental results reported in Goldsby et al. (2011), although the post-slip surface observations reported therein implied the creation of a gouge layer (of a few tens of micrometers) during fault weakening. The authors then discussed the possibility that distributed deformation (i.e., shearing) in a sufficiently thick gouge layer might prevent melting. However, further experiments performed in the presence of a thick gouge layer showed that weakening occurs in that case too, as initially proposed in Cardwell et al. (1978). Sone and Shimamoto (2009) reported slip localization in a thin section of a millimetric gouge layer but no pervasive interface melting, while Reches et al. (2010) reported spontaneous formation and thickening of a gouge layer and the development of glassy patches (i.e., solidified melt).

Shear localization is a well-documented phenomenon in granular science. In the absence of heat-related phenomena and of grain breakage, it is intimately related with the phenomenon of granular dilatancy. This concept was first proposed by Reynolds (1901), its implications on localization as well as a large number of other geological phenomena were described by Mead (1925), and its possible consequences on yield of granular materials and on earthquakes dynamics were exposed by Frank (1965). The Reynolds Dilatancy describes the necessity for a densely compacted granular material to first dilate before any other form of deformation, including shear. It means that, in addition to the steady state shear resistance of a collection of grains, a certain amount of mechanical work is needed to increase its volume against the stress applied

to it. This additional work is rendered unnecessary as soon as the sample has gained a sufficient volume to allow its shearing. This is the reason why deformation localizes in shear bands: it is much more energetically favorable to dilate the minimum amount of granular matter allowing shearing instead of the totality of the sample. The exact process leading to the appearance of shear bands is however still the topic of intense research, both experimentally (e.g., Hall et al., 2010), theoretically (e.g., Ma & Elbanna, 2018), and numerically (e.g., Tian et al., 2020). Their properties (thickness, kinematics, strength, etc.) are not yet perfectly well-understood, although it is generally agreed that they are essentially controlled by morphological properties and the particle size distribution of the granular materials.

Recent triaxial laboratory earthquake experiments illuminated that flash heating and frictional melting can be observed even on experimental faults exhibiting stick-slip events (Lockner at al., 2010, Passelègue et al., 2016, Aubry et al., 2018, 2020). In these experiments performed at confining pressures much larger than those used in high-velocity shearing experiments, pervasive melting of the interface was always accompanied by a thin (i.e., a few μm-thick) layer of fault gouge. The detailed succession of events leading the sliding surfaces to evolve to that particular stage was however unavailable to the experimental device. In the case of pervasive interface melting, the friction dependence on normal stress and sliding velocity has been formulated (Nielsen et al., 2008). Unfortunately, this model does not cover the complex transient mechanisms leading to pervasive melting of the interface. Complex interactions between the granular gouge and the molten rock are indeed expected during this weakening stage, and cannot be easily accounted for in a simple theoretical model.

To solve this issue, we document granular simulations during which thermo-mechanical phenomena occur on faults during seismic events. In Section 2, we consider that a certain layer of fault gouge pre-exists in the interface, or at least that it is created by surface abrasion and grains comminution in the very early stages of sliding, prior to the occurrence of melting. We focus on the granular behavior of the deformed gouge before any melting, since this behavior is expected to promote shear localization. In Section 3, a particular attention is put on the thermal effects related to (i) heat creation at the frictional contacts between gouge grains, (ii) heat diffusion through contacts between such grains, and (iii) heat diffusion in the medium surrounding the fault. Simulations of dry gouge in Section 2 are thus revisited with that particular focus. Melt is only introduced in the simulations in Section 4, where we investigate how the presence and a certain amount of melt in the gouge influences the accommodation mode within the interface and the rheology of the fault. Numerical results are discussed in Section 5.

2. Granular Simulation of Fault Gouge

2.1. Numerical Model

Discrete Element Modeling (DEM, Cundall & Strack, 1979) is a powerful simulation approach which represents a granular assembly as an explicit collection of rigid bodies, submitted to Newtonian dynamics and to user-defined interaction models. It has become very common in a number of scientific fields where the simulation of granular systems are of practical or academic interest. Numerical tribology makes an extensive use of this technique to simulate the rheology of tribological third bodies (i.e., discontinuous layers of material trapped in a contact, originating from damage of contacting surfaces and controlling frictional behavior, see for example Iordanoff et al., 2005, Renouf et al., 2011, and Mollon, 2015). As a straightforward extension of this concept, geophysicists have employed the same approach to simulate fault gouge in sliding seismic faults (Y. Guo and Morgan, 2007). In this section, we stick to this classical framework by considering a purely granular fault gouge. As will be elaborated in Section 4, this framework will have to be enriched to properly represent partial melting, but it is a good starting point to analyze the initial behavior of the fault before the first appearance of melt.

As shown in Figure 1, we consider a purely granular fault gouge composed of a few thousands of grains, generated with the package Packing2D (Mollon & Zhao, 2012). Their shapes are randomly and fractally generated. In the present case, the generation tool is calibrated to provide angular and facetted grains typical of comminuted gouges (Figure 1). The particle size distribution is uniform, with a median particle diameter of 1 μm and a ratio of 2 between the smallest and the largest particle sizes. This distribution is rather narrow when compared to the fractal distributions typically encountered in the field (Muto et al., 2015), and

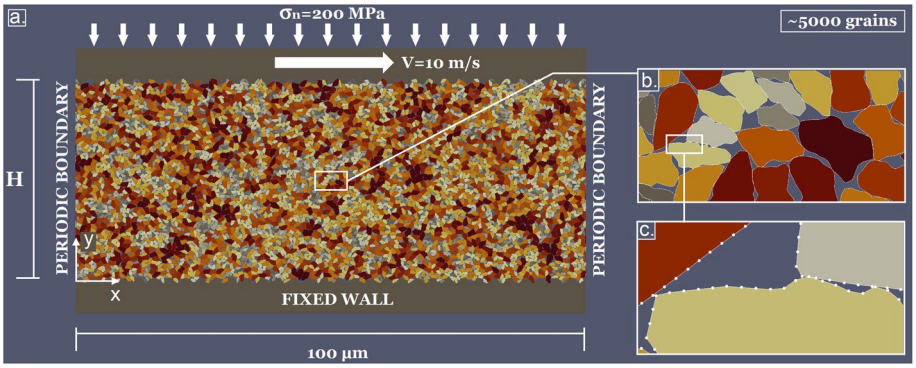

Figure 1. (a) Sketch of the model for a dry granular gouge; (b) Detailed view of grains morphologies; (c) Zoom on grains nodes and segments used by the contact algorithm.

obviously represents a simplification of real gouge material, but it allows to run simulations in a reasonable amount of time while ensuring a sufficient model size. This sample is closely packed by the generation tool in a rectangle with a length L and a height H_{gen}. It is then introduced in the simulation software MELODY2D (Mollon, 2018). This code is able to deal with such complex particle shapes by employing a robust contact algorithm based on an elastic penalization of the interpenetration between any contour node of a given body and any contour segment of another body. This provides a normal contact pressure, and an analogous tangential stiffness makes it possible to compute a tangential contact stress. Depending on the chosen contact law, this tangential stress may be limited to a certain fraction of the normal stress (Coulomb friction), or to a certain fixed value (cohesion), for example. This allows to control slip at each interparticle contact. To make this operation possible, each grain contour has to be discretized by approximately 50–100 nodes and the same number of segments. This feature provides an additional level of complexity when compared to traditional DEM simulating circular or spherical grains, and consistently improves the quality of the granular simulations, especially regarding shear localization (Mollon et al., 2020). As demonstrated in systematic experimental studies (e.g., Anthony & Marone, 2005; Mair et al., 2002), a large number of granular phenomena (friction peak, dilation, shear banding, etc.) are poorly reproduced by the traditional use of quasi-monodisperse circular/spherical particles in simulations. This has been confirmed in the past years by a large number of numerical studies (e.g., Salerno et al., 2018; Zhao et al., 2018). It is now well-established that apparent friction in a granular material increases with the irregularities of the contours of the grains, but the exact functional relation between morphology and friction is not elucidated yet. This justifies however the use of more realistic shapes in the present work, including roughness, sharp edges and somewhat planar facets. As shown in Mollon et al. (2020), accounting for all this complexity allows to reach granular friction coefficients which are closer to the experimental ones.

The main limitation of the chosen approach is its 2D character. This limitation is still rather common in the field of granular simulations, because of the very large computational cost of fully 3D simulations. This is especially true when considering particles with complex shapes, where the geometric intersection is a very computationally demanding problem. Besides, the explicit introduction of molten grains, as proposed in Section 4, is a numerical feature that does not exist yet in 3D codes. We thus have to restrict our study to plane-strain kinematics. Strangely enough, the effect of dimensionality in granular systems has been scarcely studied. It was shown in Frye and Marone (2002) that 2D granular systems exhibit friction coefficients lower that their 3D equivalent, because the energetic contribution of a large number of off-plane interactions between grains are disregarded in 2D. This drawback will have consequences on the amount of energy converted into heat in the remainder of this study, and it should be kept in mind that this energy is certainly underestimated. Regarding strain localization, however, the granular literature indicates that the major phenomena at stake are quite unaffected by the 2D or 3D character of the simulations (e.g., N. Guo & Zhao 2016; Wang et al., 2019), which explains why 2D simulations are still very common in this field of research (e.g., Tian et al., 2020).

The sample is positioned between two horizontal walls with a sinusoidal roughness designed to avoid wall-slip effects since grain accommodation within the gouge is our primary interest. Periodic boundary

conditions are applied on the two lateral faces of the sample, allowing deformation at large slips. The lower wall is fixed, while a vertical downward stress of 200 MPa is applied to the upper wall to simulate confining pressure at typical seismogenic depths. During this stage, the contact model between the grains is frictionless in order to maximize the compaction of the sample. A volume fraction of 0.86 is obtained, with a corresponding gouge thickness H. Volume fraction in this paper refers to the proportion of the apparent volume of the gouge occupied by solid or liquid matter (but not gaseous). After compaction, grain contacts are driven by a frictional model without cohesion (Mohr-Coulomb type, friction coefficient of 0.8). This large value follows the recommendations of Mollon et al. (2020) and aims to compensate the smoothing of the grains surfaces induced by their discretization. The upper wall is submitted to a horizontal velocity of 10 m/s (i.e., a velocity higher than typical sliding velocities in earthquakes in order to accelerate the simulation process), while its vertical motion remains free in order to accommodate possible dilation or compaction in the sheared gouge. Rotation is prohibited, however, and the upper wall remains horizontal. The inertial number I of the granular system was introduced in the field of granular physics (MiDi, 2004) as a way to characterize granular flow regimes. It is a dimensionless number which compares the unbalanced (i.e., inertial) force on a grain with the value of the forces it receives through its contacts, in relation with the stress level in the sample. With the typical grain size, grain density, normal stress, and shear rate of this study, the inertial number is close to $I = 9 \cdot 10^{-4}$, which classifies it in the category of dense quasi-static shear flows (Forterre & Pouliquen, 2008). This means that the inertial forces are negligible, that the sample is very close to static equilibrium at any time of the simulation, and that shear rate has no significant effect on the grains kinematics.

2.2. Influence of the Dimensions of the Gouge Layer

In order to determine the size of the representative volume element (RVE), several values of the model length L are first tested, ranging from 20 to 200 μm, with a constant thickness H of about 45 μm. Below the optimal model length $L = 100$ μm, the friction coefficient (defined as a ratio of shear stress and normal stress) strongly fluctuates along simulated time, indicating that the system is too small to be statistically reliable. Hence, the model length is kept constant and equal to 100 μm.

Four gouge models are built with compacted thicknesses of 9, 22, 45, and 90 μm, containing respectively 1,000, 2,500, 5,000 and 10,000 grains. The time-series of the friction coefficients obtained for these four cases are provided in Figure 2. All these simulations show that sliding first induces a strong friction peak of 0.75–0.8, followed by a linear slip-weakening of the fault, and by a friction plateau where a frictional steady-state has been reached. This initial peak is related to the energy spent by the sample to dilate against the applied normal pressure (i.e., break the initial compacted configuration of the grains) and reach a lower density at which shearing is possible. The weakening part is very short for the less thick gouge, but gets more delayed when the thickness increases. Steady state friction is concomitant with the end of the sample dilation. The cases $H = 45$ μm and $H = 90$ μm exhibit similar weakening behaviors.

2.3. Steady State Friction and Kinematics

Since we are interested in fault weakening induced by partial melting, we disregard any transient phenomenon related to the very onset of sliding, and focus on the steady state behavior of the simulations. Indeed, the melt-related weakening is a delayed phenomenon, which occurs after a sliding distance that is much larger than that concerned with the initial dilation. In the steady state, the average friction of the dry (i.e., not melted) gouge μ_d is only moderately influenced by the model thickness: it is equal to 0.495 for the 9 μm-thick fault, and stabilizes at 0.460 for thicknesses equal to or larger than 45 μm. Thicker faults also tend to stabilize the evolution of the friction coefficient and to reduce its fluctuations.

However, it appears that most of the slip is accommodated in the central part of the layer in the 45 μm-thick case, and that some areas close to the walls remain almost undisturbed (Figure 3). This phenomenon is even more present in the 90 μm-thick case, where more than one half of the gouge thickness remains undeformed during shearing. In the 90 μm-thick case, the sample only dilates in the upper part accommodating shearing and reaches an average volume fraction of 0.77 in the shear band: no shear takes place in the lower

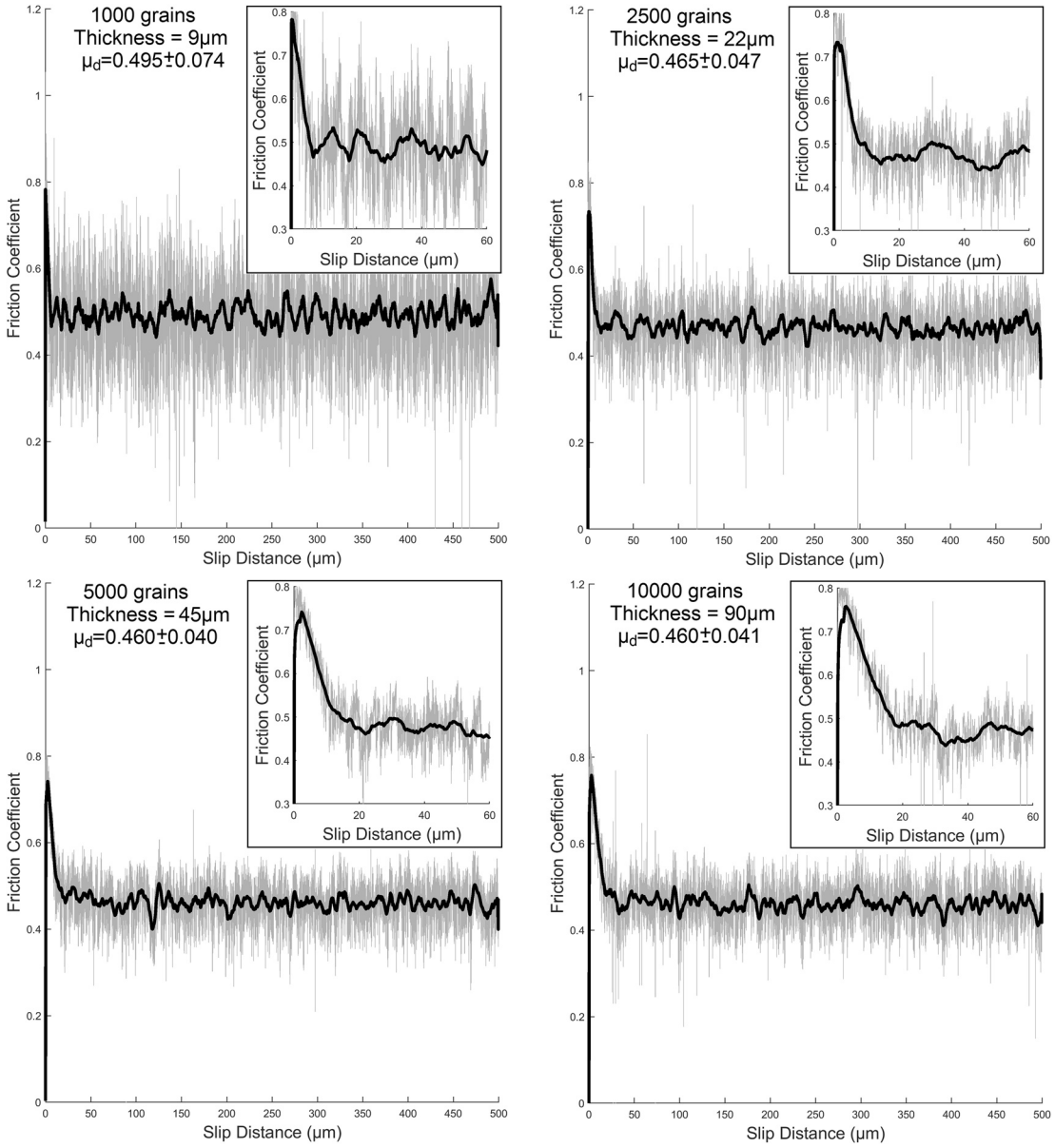

Figure 2. Friction coefficients as functions of sliding distance for four different gouge thicknesses; gray lines: raw numerical data; bold black lines: moving average; Inserts: first 60 μm of slip.

part and indeed the sample is still in its initial state of compaction (i.e., volume fraction about 0.86). From this calibration, we conclude that the shear localization thickness of the granular medium is close to 40 μm, in good agreement with numerical and experimental estimates which usually range between 15 and 50 times the median grain size (Mollon et al., 2020; Torsedillas et al., 2004). Thus, all the remaining simulations described in this paper will adopt an initial gouge thickness of 45 μm.

A more detailed view of the accommodation mechanism is provided in Figure 4 for the 45 μm-thick sample. Key local quantities are averaged along the horizontal direction in order to extract instantaneous vertical profiles. The figure shows that local shear rate keeps a rather constant maximum value (close to 5.10^5 s^{-1}) but that the locus of this maximum evolves in time. Hence, the instantaneous shearing profile is very sharp (at a given time, most of the shearing occurs in a thickness smaller than 10 μm). The idea of active sites shifting rapidly within a broader zone postulated in Rice (2006) is thus confirmed by our numerical results.

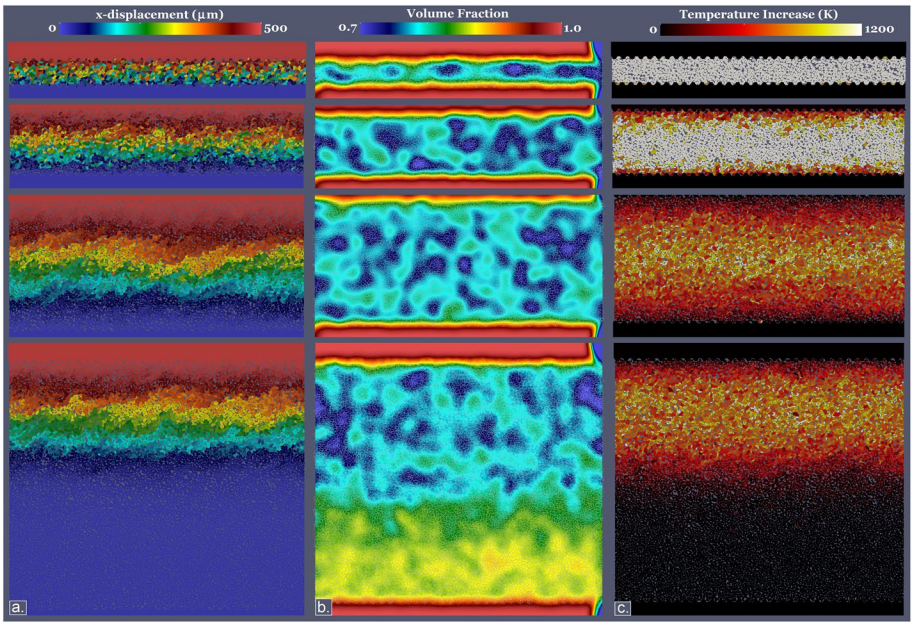

Figure 3. Views of the models with four different gouge thicknesses (H = 9, 22, 45, and 90 μm, from top to bottom) after 500 μm of sliding—Shear direction provided in Figure 1; (a) Final Horizontal Displacement (lower wall remains still, upper wall slides on 500 μm, grains in the middle have horizontal displacements ranging from 0 to 500 μm); (b) Final Volume Fraction; (c) Heat production in grains, expressed as temperature elevations in adiabatic conditions (No melt is considered here, despite the large temperature elevations, see Section 3).

3. Thermal Aspects

3.1. Adiabatic Temperature Increase

Simulating fault gouge melting requires a temperature field within the gouge and the surrounding rock. A first step to achieve this issue was to implement a temperature tracker in MELODY to evaluate the heat produced by friction between grains. The tracker records frictional dissipation on contacting grains and assumes all the dissipated energy is converted into heat, disregarding any other energy sink. Each grain in a contacting and sliding pair undergoes a temperature increment:

$$\Delta T = \frac{0.8vF \cdot \Delta t}{2} mc_p \tag{1}$$

where Δt is the time step duration; v is the grains pair mutual sliding velocity; F is the normal force supported by the contact; m is the grain mass; c_p is material heat capacity; and 0.8 is the interparticle friction coefficient. The field of temperature in the grains is considered as homogeneous. Figure 3 shows that heat creation is restricted to the areas where shearing takes place, and that higher temperatures are reached after a given sliding distance if the gouge layer is thinner. Hence, temperature increase is intimately related with shear localization. Heat creation is distributed over the whole thickness of the sheared layer, but is maximum in its center.

3.2. Contact Conductivity Calibration

Heat creation is very heterogeneous in the grains of the sample: under these assumptions, very close grains can have very different temperatures, which does not seem right (Figure 3). Since mechanical contacts exist between touching grains, we shall expect a certain amount of heat diffusion through them. The problem of heat flux through mechanical contacts has been investigated in several studies (Madhusudana & Ling, 1995). However, in the present case, the contact configurations are both complex (because of the angularity of the grains) and simplified (because of their limited discretization). Hence, we use a constant thermal conductivity k_c for all the intergranular contacts, whatever their geometry and supported load.

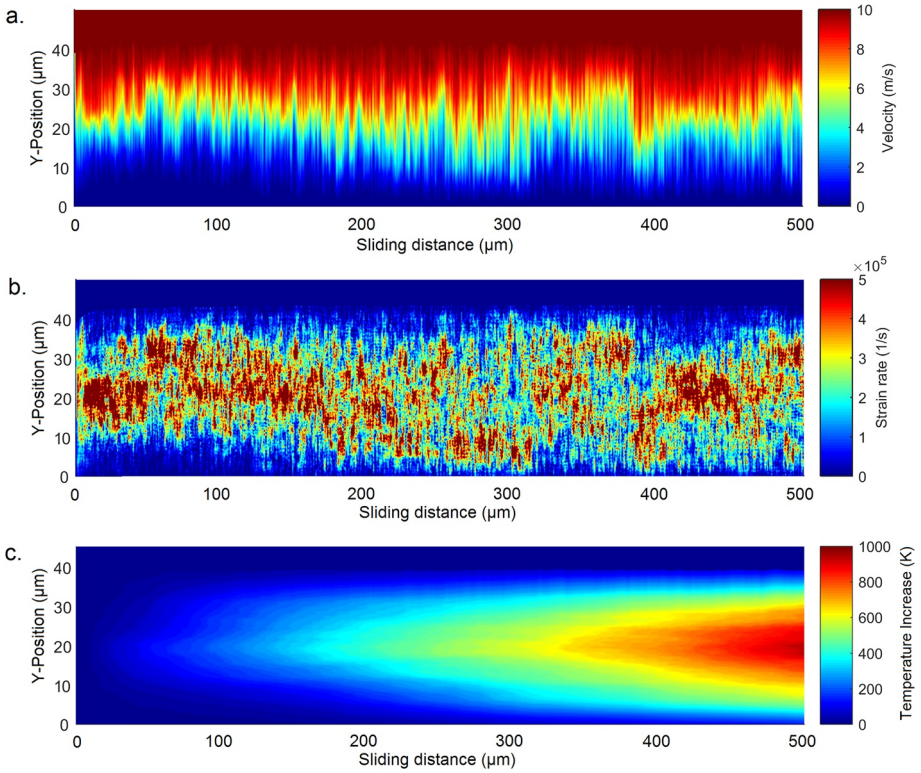

Figure 4. Evolution of key quantities for the reference model during 500 μm of sliding. At a given time, each quantity is averaged on horizontal slices in the sample to compute a vertical profile along y (Figure 1), and these profiles are plotted here as a function of the sliding distance; (a) Horizontal Velocity; (b) Shear Rate; (c) Heat production expressed as a temperature increase in adiabatic conditions (see Section 3).

To calibrate this conductivity, we consider a situation where the gouge layer is at rest in its initial state. In this preliminary calibration stage, no motion is imposed on the upper wall of the simulation. A thermal network based on the initial compacted state of the granular sample is built. We consider each grain as a node (defined by its mass and its heat capacity), and each contact as a link between two nodes. A detailed view of this network is provided in Figure 5. A given node i has a temperature T_i, and the heat flux through the contact between any two contacting nodes i and j is given by:

$$q_{i\to j} = k_c \cdot \left(T_j - T_i\right) \tag{2}$$

The term k_c in this equation is a 1D contact conductivity (unit W.K^{-1}) which provides the heat flux through a given mechanical contact (if it exists), and should not be confused with bulk contact conductivity of a given medium (unit W m^{-1} K^{-1}). To establish a vertical heat flux within the thermal network, we impose a global temperature gradient of 1000 K over a thickness of 30 μm (Figure 5). In the central part of the layer (black dots in Figure 5), nodes are let free to reach their equilibrium temperature. Thermal equilibrium is reached by using a simple heat diffusion numerical scheme based on Equation 2, after a certain relaxation time. In this case, we find that stabilization of the thermal system (in the absence of any motion of modification of the contact network) is reached after about 1 ms. The equilibrium temperature field is close to a linear temperature profile (Figure 5). Assuming k_c = 1 W K^{-1}, we obtain at equilibrium a constant total heat flux (integrated on all the contacts between black and blue areas, Figure 5) of 5.969.10^7 W/m^2. Under the imposed gradient of temperature, this leads to a macroscopic thermal conductivity of 1.7908 W m^{-1} K^{-1}. In order to reach the thermal conductivity of intact Westerly granite (about 2.9 Wm^{-1}K^{-1}), we would need a calibrated contact conductivity of 1.6194 W K^{-1} (obtained by simple linearity of the heat conduction problem). However, thermal diffusivity reported in Vosteen and Schellschmidt (2003) for granite gouge are close to 0.7.10^{-6} m^{2}s^{-1}, which is smaller than typical values of about 1.10^{-6} m^2 s^{-1} for bulk

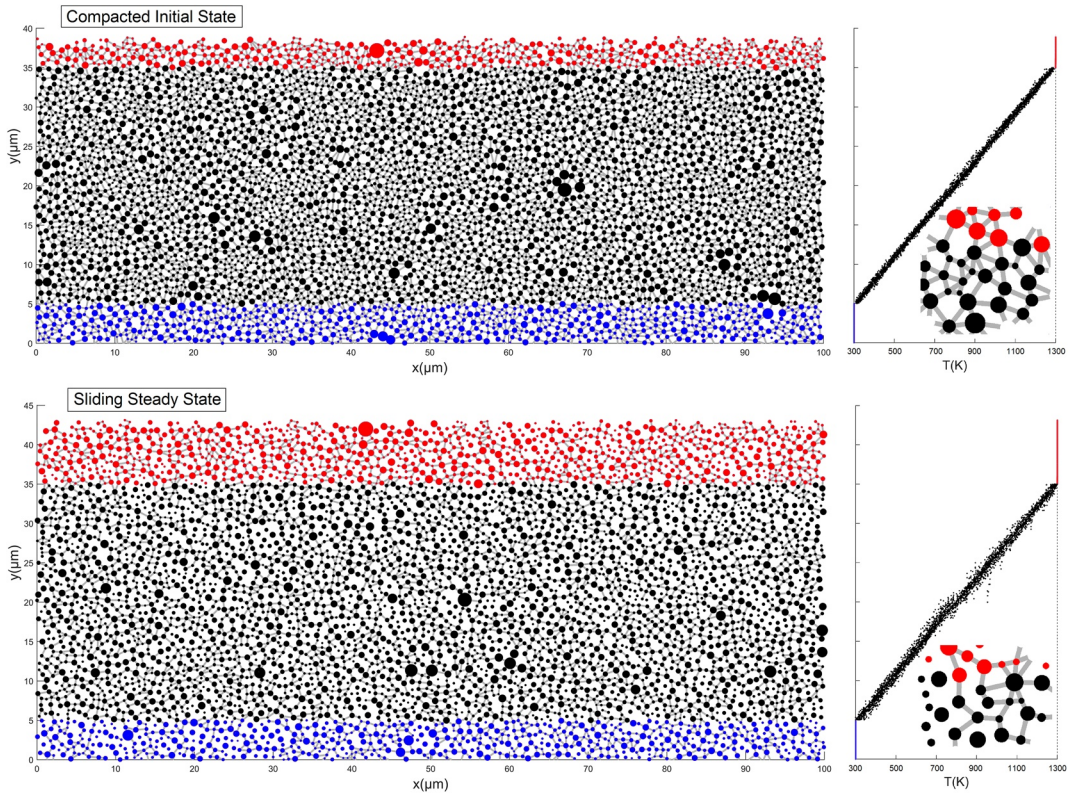

Figure 5. Calibration of intergranular contact thermal conductivity under a stabilized vertical heat flux. Left-hand panel: Thermal network (size of the dots indicates the mass of each grain, gray lines indicate heat-conducting mechanical contacts, red dots (above $y = 35$ μm) are grains set at a constant temperature of 1300 K, blue dots (below $y = 5$ μm) are grains set at 300 K, and black dots are grains which remain free to evolve to their equilibrium temperature); Right-hand panel: Temperature profiles at thermal equilibrium and zoom on a local area of the thermal network; Top: initial compacted state; Bottom: after 500 μm of sliding (gouge thickness increased because of granular dilatancy, since thermal expansion of grains is disregarded).

granite (Aubry et al., 2018; Passelègue et al., 2016). Therefore, to match the value measured by Vosteen and Schellschmidt (2003), we adjust the contact conductivity to $k_c = 1.1336$ W K^{-1} in our simulations. If we repeat the same thermal simulation, but considering the thermal network as it has evolved after 500 μm of sliding, the heat flux obtained with the calibrated contact conductivity is close to 0.39 times that of the initial state (Figure 5). This means that the dilation and loss of many contacts induced by the shearing lower the overall thermal conductivity of the gouge layer by a factor 2.5, which is considerable.

3.3. Heat Diffusion and Temperature Variability

One-dimensional thermal networks are connected to top and bottom boundaries (with appropriate conductivities and heat capacities based on bulk granite) to allow heat diffusion in the medium surrounding the fault (Figure 6). It was confirmed experimentally in Mair and Marone (2000) that this 1D simplification of the heat diffusion was licit. The importance of this diffusion has been confirmed experimentally in Yao et al. (2016), showing that a large conductivity of the surrounding medium is prone to limit the amount of melt appearance. The granular simulations reported in Section 2 are then revisited based on the mechanical data stored on disc in order to account for heat diffusion through contacts, using the contact conductivity calibrated in the previous sub-section. After setting the initial temperature of all the bodies to 300 K, this second pass accounts, at each time step, for the evolving contact network within the gouge (and between the grains and the walls) as described in Section 3.2, and for the created thermal energy obtained following the method described in Section 3.1. Obviously, it is not possible to record on hard drive the contact network at each time step of the mechanical simulations. This approach remains however correct thanks to a sufficient

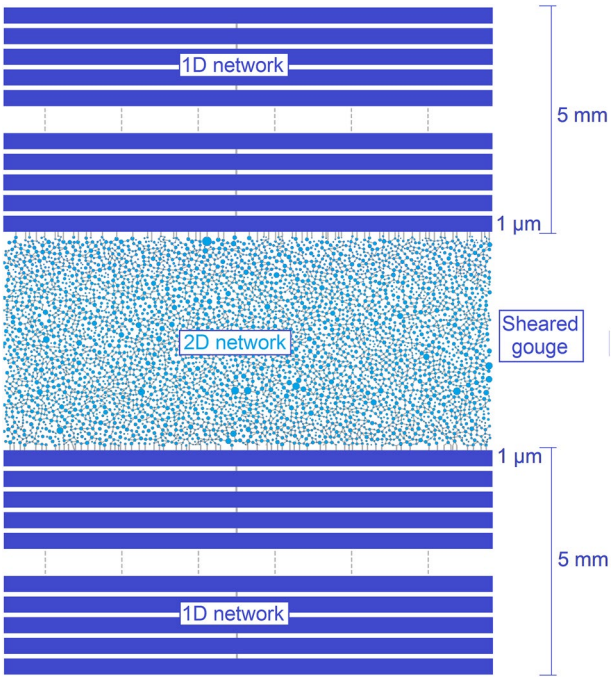

Figure 6. Mixed 1D-2D thermal network for the transient heat diffusion simulation.

network sampling rate, and thanks to the fact that we are dealing with a dense quasi-static flow. In contrast with a collisional granular flow, the typical contact life-time is rather long and interpolation is licit. Hence, both conductive (though the evolving network of contacts) and advective (through grains motions) heat fluxes are considered here. A major interest of this approach is that we can simulate several sliding velocities from the same initial granular simulation. Since the flow is quasi-static (i.e., near mechanical equilibrium at any time of the simulation), the time considered in the granular simulation is not physical, and is just an evolution parameter. When applying the heat diffusion as a second pass, it is therefore possible to modify the physical time without running the granular simulation again. It should be stressed, however, that the temperature elevation that is computed here does not have any feedback on the mechanical results, since simulations of dry gouge are used as a mechanical basis for this evolving thermal network. Melt is only introduced in simulations in Section 4.

The results of the simulations are summarized in Figure 7. For a sliding velocity of 10 ms^{-1} (Figure 7a), a progressive temperature increase, with a maximum value close to the center of the gouge layer is observed. The diffusive case leads to a profile with a lower maximum value and a much lower variability. Temperature profiles across the gouge thickness after 500 μm of sliding for sliding velocities ranging from 0.1 to 10 m s^{-1} are shown in Figure 7b. Since the heat created is purely proportional to the sliding distance (and not to sliding velocity), the only difference between these cases is the time allowed for heat diffusion. It demonstrates that sliding velocity has a considerable influence on the temperature profile in the gouge layer, with maximum values ranging from 500 to 1150 K at the end of the simulation (1250 K in adiabatic conditions). These values, however, are not to be mistaken with steady-state temperatures in the gouge layer since the temperature profile keeps increasing with sliding (Figure 7a). In the case of the largest sliding velocities considered here (e.g., 10 m/s), reaching this steady state would require sliding distances that are out of reach for our granular simulations.

In order to quantify the variability of the grains temperatures, temperature statistical distributions (corrected by the average temperature in the horizontal layer for each grain) after 500 μm of sliding, are calculated both for the adiabatic and diffusive cases (Figure 7c). The distribution for the adiabatic situation is slightly skewed and is very broad, while that of the diffusive case is quasi-Gaussian and much narrower. The standard deviation obtained from this distribution ranges from 4 K in the case of low sliding velocities to 18 K for fast sliding. It is thus evident that large sliding velocities can promote larger temperature heterogeneities within the sample, largely influencing the onset of melting (Figure 7d).

4. Granular Simulation of Fault Gouge Melting

4.1. Model Description

Knowing the melting point of the minerals composing the simulated gouge, it is possible to predict the time and location of first appearance of rock melt in the gouge layer. From that point, however, the previous results are useless because the presence of molten rock is expected to considerably modify the local rheology of the gouge, altering its frictional behavior and thus the amount of heat production. To go beyond that point, it is thus necessary to explicitly simulate the presence of melt in granular simulations. The particular case of melting in fault gouge is complex to model since, (i) the gouge layer is a ternary combination of solid rock, molten rock and porosity (Aubry et al., 2018), (ii) the melt fraction can take very different values (from a little melt in the granular assembly to a few solid grains inside a liquid layer), (iii) this fraction evolves in space and time depending on the temperature distribution, and (iv) the shear rate is very high.

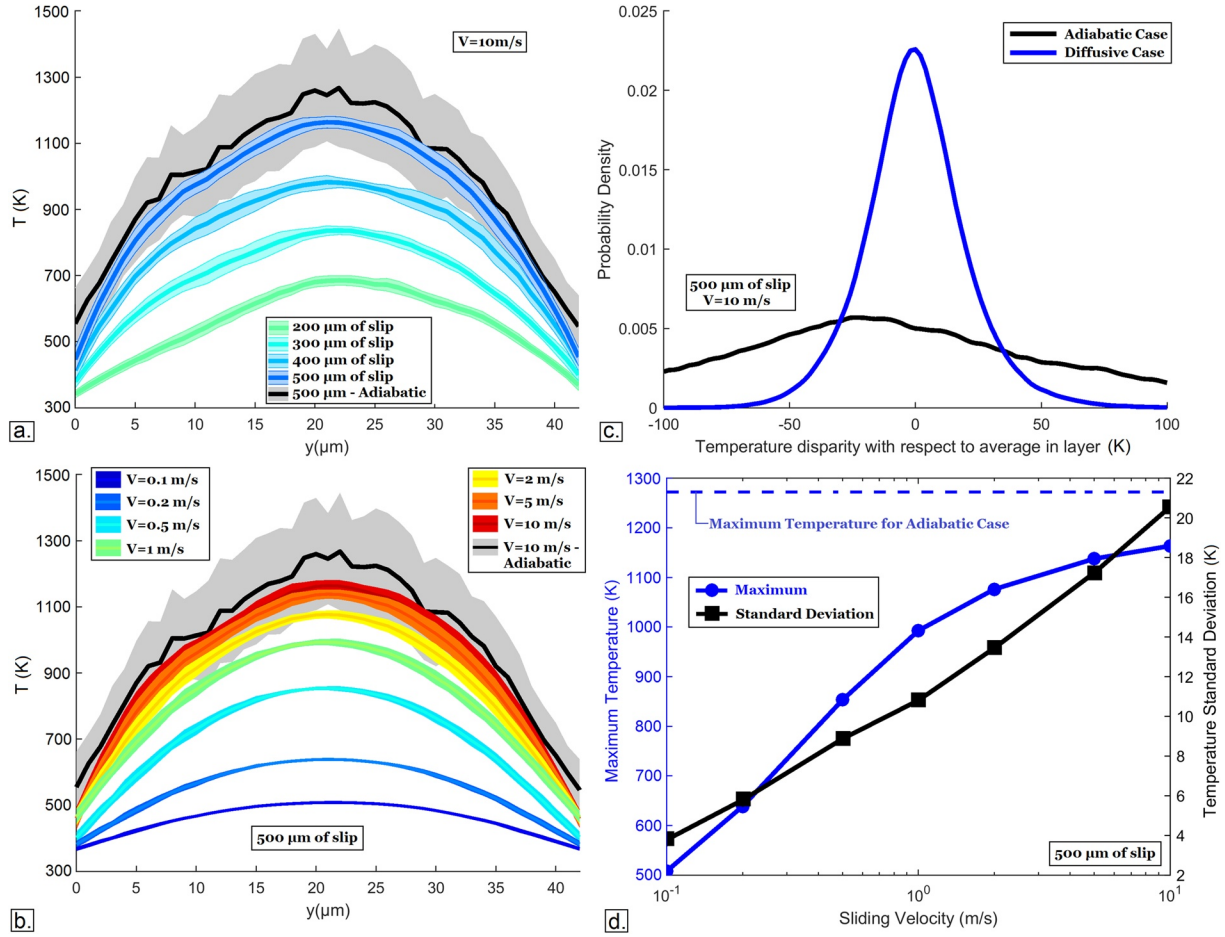

Figure 7. Thermal results; (a) Temperature profiles across the gouge thickness (±one standard deviation) at several sliding distances, for a sliding velocity of 10 ms^{-1} (adiabatic case in gray); (b) Temperature profiles across the gouge thickness (±one standard deviation) after 500 µm of sliding, for different sliding velocities (adiabatic case in gray); (c) Statistical distributions of the grains temperatures (corrected by the average temperature in their horizontal layer) in the adiabatic and diffusive cases; (d) Maximum value and standard deviation (with respect to the average in horizontal layer) of the grains temperatures at different sliding velocities.

Here, the molten grains are modeled as highly compliant, visco-elastic, frictionless, incompressible bodies. This approximation retains a large part of the physics of the problem (the soft, viscous and incompressible character of the melt) and provides an approximate model of the local lubrication brought by the molten rock into the initially granular gouge. MELODY simulates such compliant bodies using a multibody mesh-free approach (Mollon, 2018). Each body is discretized by a large number of field nodes which carry the degrees of freedom in displacement. The equations of continuum mechanics extended to finite strains are then solved on each grain using a weak-form. The deformed bodies can interact with each other, using the contact algorithm described in Section 2. The overall dynamic simulation is solved in time by an explicit solver, just as in classical DEM. This approach was already successfully applied in tribology and in granular physics (Mollon, 2019). It is obviously a coarse approximation of the liquid phase in the gouge, since the soft grains cannot readily flow between more solid particles, but it is the most efficient way to implement a liquid-like behavior in the present framework.

In the case of solid grains, heat creation is estimated by transforming all the mechanical energy by inter-granular frictional contacts into heat (Equation 1). However, soft and melted grains do not dissipate energy at their boundaries, because a frictionless contact law is used for any contact implying a soft grain. For these particular grains, all the energy dissipation is provided by the viscous part of the constitutive law implemented in each grain. Hence, to evaluate heat creation while ensuring energy conservation in each soft grain, we simply transform all the mechanical energy dissipated by viscosity into heat.

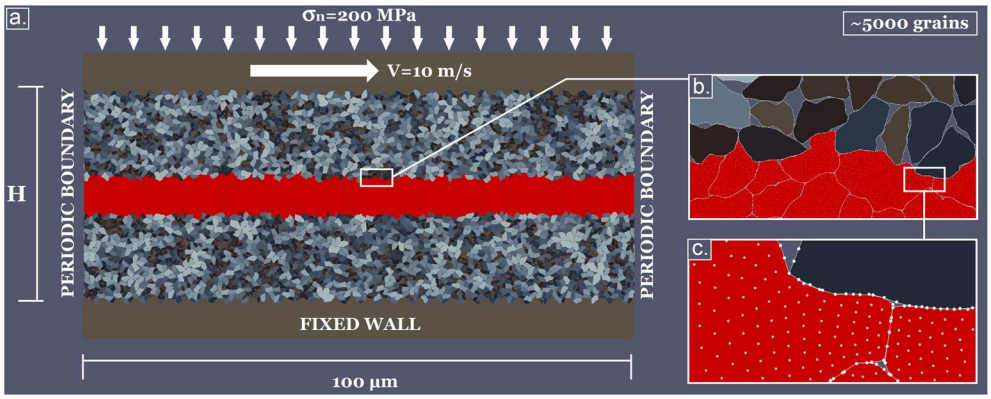

Figure 8. (a) Sketch of the model for a granular gouge with partial melting (completely melted central layer in this case, molten grains in red); (b) Detailed view of grains morphologies; (c) Zoom on grains field nodes, and on nodes and segments used by the contact algorithm.

A typical model is shown in Figure 8. In that specific case, we consider complete melting (i.e., a melt proportion $\varphi_m = 1$) in a central layer of thickness $H_m \approx 8\,\mu m$. The simulation process is identical to that of Section 2 (i.e., compaction under 200 MPa, stabilization, and shearing at a sliding velocity of 10 ms^{-1}). This simulation shows that the porosity is almost reduced to zero in the molten layer, because the soft grains deform immediately under the confining stress, while remaining quasi-incompressible. This is made possible by the relative motion of the field nodes within each body (Figure 8, lower-insert).

4.2. Influence of the Melt Fraction

As the first molten grains seem to appear in the central area of the gouge layer, a set of numerical simulations with a constant melt layer thickness but a varying melt proportion within this layer is performed in order to cover the whole range of rheologies of the gouge layer (Figure 9). We thus artificially place a controlled proportion of molten grains in the central part of the gouge layer. This arbitrary choice is necessary because the numerical code is not able to simulate melting (i.e., the transition from rigid to soft grain) explicitly. We thus consider steady states of interface melting, which allows to collect enough data to obtain statistically relevant models, but disregards the transient effects of the melting process. Molten grains are located in the central

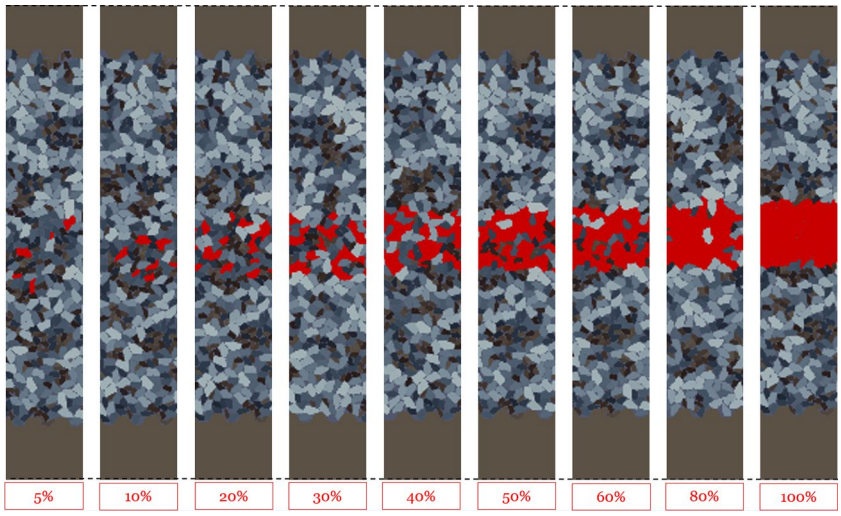

Figure 9. Illustrative vertical slices of the simulations performed with a varying melt proportion φ_m, from 5% to 100%.

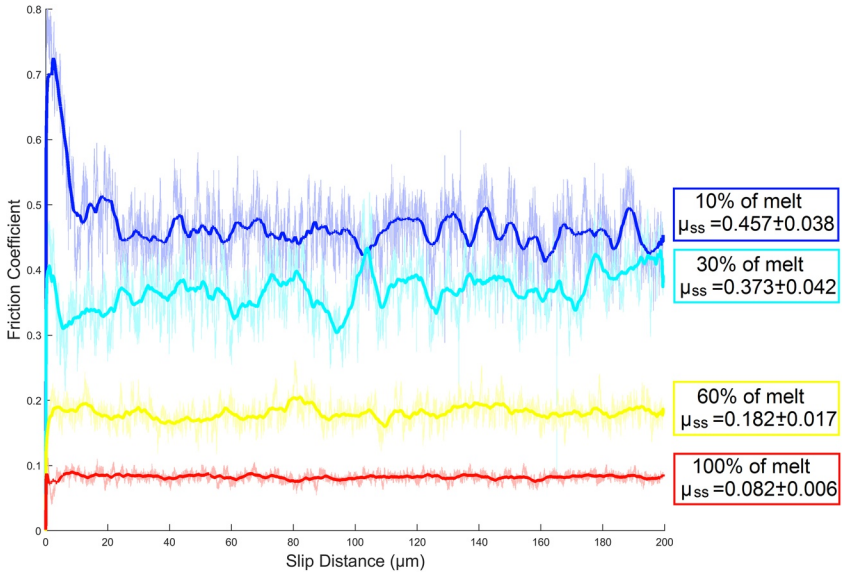

Figure 10. Friction time-series for four different fractions of melt in the central layer; thin lines: raw numerical data; bold lines: moving average.

10 μm (≈8 μm after compaction) because the thermo-mechanical results of Section 3 (Figure 7) indicate that the first molten grains will likely appear in the central area of the gouge layer. The onset of melting will thus involve interactions between a partially molten layer in the center and dry granular layers around it.

Time series of the friction coefficients obtained for four different proportions of melt in the central layer (10%, 30%; 60% 100%) are shown in Figure 10. The progressive increase of the proportion of melt tends to reduce the intensity of the initial friction peak (meaning that it progressively suppresses dilatancy), and to reduce the steady-state friction coefficient (from 0.457 for 10% of melt to 0.082 for 100% of melt). It also stabilizes the friction signal by reducing the intensity of its fluctuations. The first part of the curves is rather irrelevant since it correspond to artificial initial states with prescribed amounts of melt prior to sliding. In the remainder of this study, only the steady-state part of these curves is used for analysis.

Figure 11 provides the spatial distributions of the molten grains, the field of horizontal displacements, and the field of temperature increases (in the adiabatic case) for the same four cases. This temperature increase includes both the energy coming from the frictional contacts between solid grains and the viscous dissipation in soft grains. For low melt proportion, some molten grains are transported in the transversal direction during shearing, while this is not observed for the fully molten layer. Likewise, the mobilized thickness over which a certain amount of shear is accommodated is much larger at low melt fractions (i.e., close to the dry case, at $\varphi_m = 10\%$, for example), but is fully localized in the case of a fully molten layer (φ_m=100%). This trend, combined with the friction curves (Figure 10), leads to a surprising result in terms of heat generation. As shown in Figure 11 (right-panel), an intermediate value of φ_m (∼30%) maximizes the adiabatic temperature increase in the grains. For lower melt fractions (e.g., $\varphi_m = 10\%$) the heat creation is less localized, while it is more localized but less intense for larger melt fractions (e.g., $\varphi_m = 60\%$), owing to a lower apparent friction coefficient.

Figure 12 provides the fields of volume fraction (i.e., proportion of the fault volume occupied by the solid and the molten grains) for the same cases. The case with 10% of melt shows a very similar behavior to a purely dry gouge, i.e., shearing and dilation in a broad shear band. When the melt fraction is increased to 30%, dilation takes place in a less broad area. For higher melt fractions, no dilation takes place in the granular part and porosity is close to zero in the melt layer.

Shear rate profiles across the fault (averaged on horizontal slices) are provided for different melt fractions in Figure 13, illustrating the progressive localization promoted by the presence of melt. The accommodation zone ranges from about 40 μm for $\varphi_m = 0\%$ (purely granular localization) to about 8 μm for $\varphi_m = 100\%$ (shear

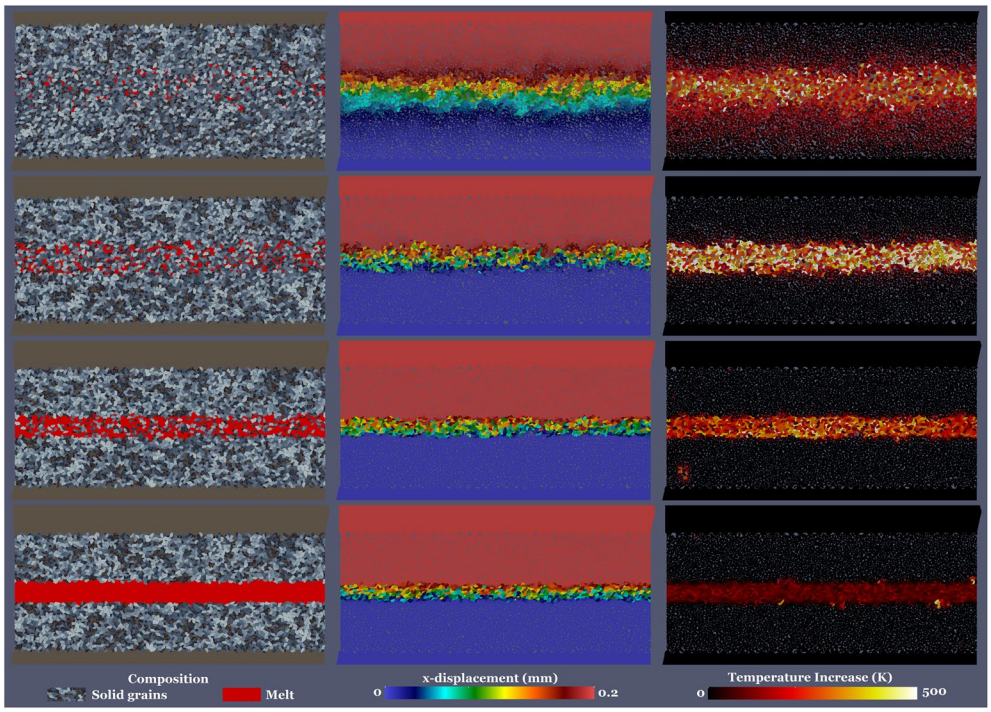

Figure 11. Views of sliding faults with partial melting in the central layer after 200 μm of sliding distance; Left-panel: distribution of molten grains, in red; Central panel: horizontal displacement of each grain; Right-panel: Temperature increase in each grain (adiabatic case). Top to bottom: 10%, 30%; 60%; 100% of melt in the central layer.

restricted to the liquid layer). In this latest case, the steady state apparent friction coefficient provided in Figure 10 combined with the shear rate averaged on the melt layer leads to an equivalent viscosity of the simulated melt layer $\eta_m = 10.0$ Pa.s. This value is close to the lower range of values measured on carbonated rocks, see for example (Kono et al., 2014).

5. Discussion

5.1. Friction and Rheology

Based on the simulations, steady-state fault friction can be interpreted following:

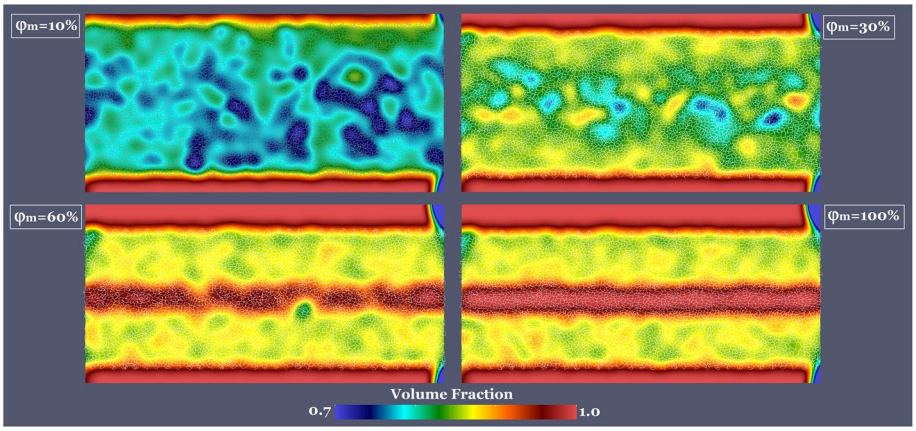

Figure 12. Volume fraction in sliding faults with partial melting in the central layer after 200 μm of sliding distance.

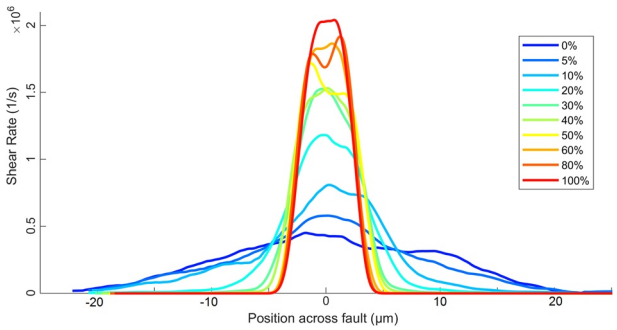

Figure 13. Shear rate across the fault for different values of the melt proportion.

$$\mu = \frac{\dot{W}_c + \dot{W}_v}{\sigma_n \cdot \Delta V} \tag{3}$$

where ΔV is the applied sliding velocity; $\dot{W}_c$ is the average rate of mechanical work dissipated by contacts between solid grains and $\dot{W}_v$ is the average rate of mechanical work dissipated by the viscosity in molten grains. These two work rates can be extracted from a given simulation by techniques analogous to those used to compute adiabatic temperature increase in each grain in Section 3. Following the logic presented in (Mollon, 2019), we can compute μ_c and μ_v, the apparent friction coefficients related to the Coulomb and viscous contributions acting in the gouge layer, respectively:

$$\mu_c = \frac{\dot{W}_c}{\sigma_n \cdot \Delta V} \tag{4}$$

$$\mu_v = \frac{\dot{W}_v}{\sigma_n \cdot \Delta V} \tag{5}$$

These contributions are plotted as a function of the melt fraction φ_m for the whole numerical campaign (Figure 14). This decomposition should not be seen as the addition of two coefficients of friction in the Coulomb sense, but rather as a simple way to characterize the share of energy dissipation taken by each phase. Two end-members can be identified: (i) the case $\varphi_m = 0\%$, which strictly corresponds to Coulomb friction, with a total friction coefficient of 0.460; and (ii) the case $\varphi_m = 100\%$, which corresponds to purely viscous friction with a total friction coefficient of 0.082. We observe that numerical results close to this second end-member are in good accordance with the well-known Einstein formula (Coussot & Ancey, 1999), which is valid for highly diluted suspensions of rigid grains in a Newtonian fluid. Adapted to the notations of the present work, this formula follows:

$$\mu = \mu_v \cdot \left(1 + 2.5\left(1 - \varphi_m\right)\right) \tag{6}$$

For melt fractions below 70%–80%, however, results logically deviate from this simple law (Equation 6) because interparticle dry friction comes into play.

It is instructive to compare the simulation results to a simple linear mixing law that would state that the contribution of each phase be proportional to its volume fraction in the mixture. It would thus give:

$$\mu_c = 0.460 \cdot \left(1 - \varphi_m\right) \tag{7}$$

$$\mu_v = 0.082 \cdot \varphi_m \tag{8}$$

Although correct at the two end-members, this simple law does not appear to fit correctly the data (Figures 14b–14d). The linear mixing model overestimates the contribution of interparticle friction in the response of the mixture to shearing (Figure 14b). As the proportion of molten grains increases, the remaining dry grains appear to dissipate less energy than their share. This is especially the case when reaching melt contents around 50%, for which the contribution of dry grains to friction becomes very low while they still are rather numerous in the partially molten layer. In addition to reducing the number of solid grains, melting also seems to reduce the frictional efficiency of grain contacts.

In contrast, the linear mixing model underestimates the energy dissipated by viscous deformation of the molten grains (Figure 14c). For melt fractions from 20% to 50%, where the amount of molten grains is still rather low, viscous dissipation contributes to the overall friction coefficient close to 0.15–0.18. This is twice larger than the friction obtained for a fully molten layer. The interplay between rigid grains and melt leads to local shear rates which are much larger than the average one (Figure 15). When adding both contributions to friction, an interesting deviation from the linear mixing model appears (Figure 14d). Instead of a

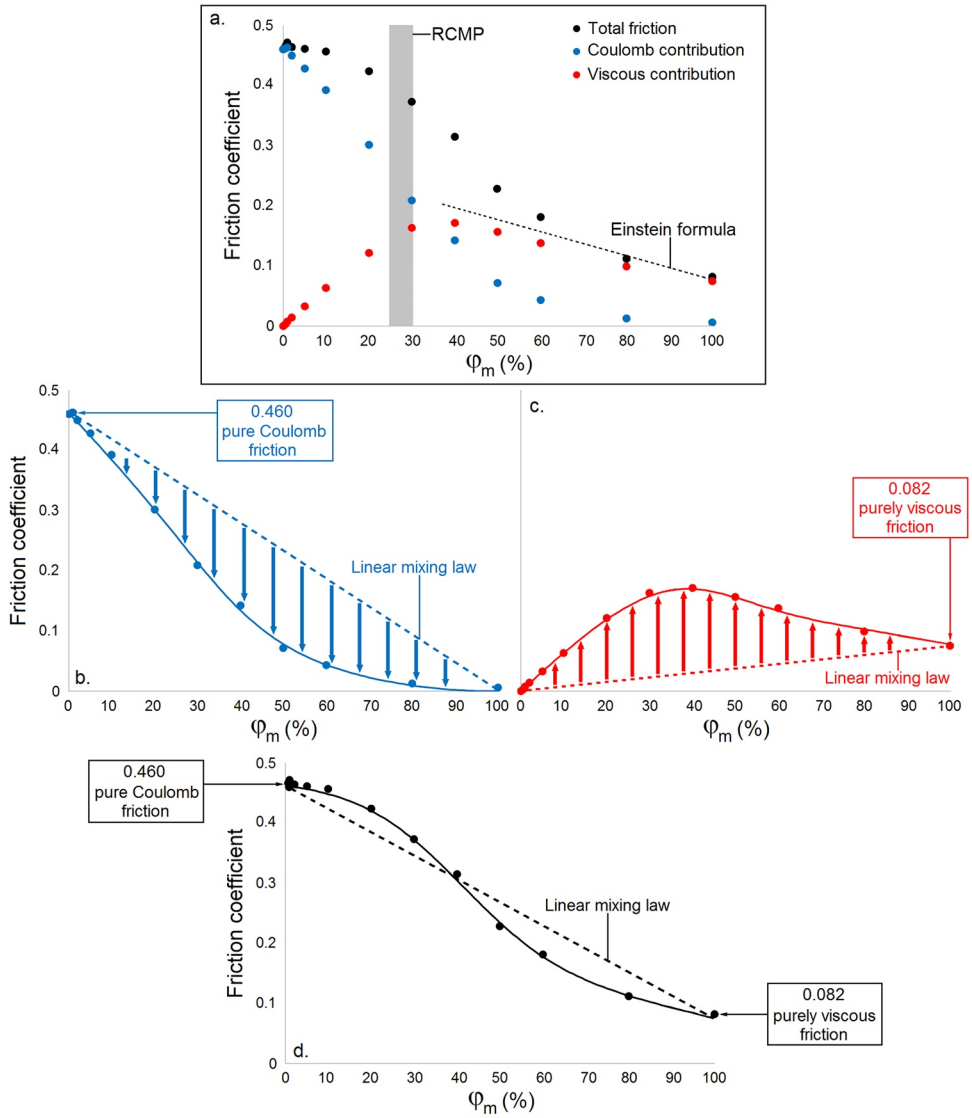

Figure 14. Influence of partial melting on friction coefficient; (a) Numerical results; (b) Coulomb contribution to friction; (c) Viscous contribution; (d) Total friction; Dots indicate simulation data, solid lines are just guides to the eye, dotted lines in (b–d). are a simple linear mixing law.

linear decrease of friction with the increase of φ_m, numerical results suggest a sigmoid shape, with a more sudden drop for intermediate values of φ_m (~30–60%). We note that this result is in agreement with values of the Rheological Critical Melt Percentage (i.e., the melt fraction above which a cristal-bearing magma departs from its solid state and starts behaving as a viscoplastic fluid), estimated by Arzi (1978) to be of the order of 25%–30% (Figure 14a). The agreement extends to the general shape of the weakening curve beyond 30%, which is reported experimentally in Costa et al. (2009) to approach a decreasing exponential. It should be noted, however, that such results were obtained in a rather different context (i.e., slow shearing of bulk crystalline rock deformed at very low strain rates, for volcanology applications). Nevertheless, the behavior obtained in our simulations is likely to promote a slightly more delayed but also more prompt fault weakening.

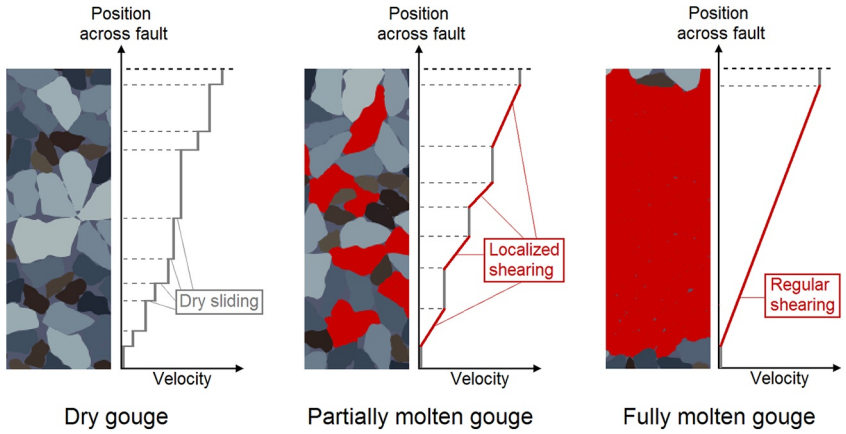

Figure 15. Sketch of the accommodation modes for dry, partially molten, and fully molten gouge (highly simplified representation disregarding rotations and vertical motions of grains).

5.2. From Numerical Modeling to Experiments: The Concept of Flash Heating and Frictional Melting

Simulation results in intact gouge prior to melting are in good agreement with several experimental and theoretical studies describing shear localization in a thin and compacted gouge layer (Platt et al., 2014; Rice et al., 2014; Sone & Shimamoto, 2009). However, this study questions the way seismic faults subjected to flash heating and frictional melting are conceptualized in many theoretical models. Most of these models indeed rely on the concept of "asperity", seen as a geometrical feature that bears a very large proportion of the normal load and therefore concentrates heat creation. However, all experimental evidences point toward the fact that bare rock surfaces are almost immediately separated by a layer of fault gouge because of the degradation of the sliding surfaces (Aubry et al., 2018, 2020). The size of the asperities is closely related to confining pressure and the average contact lifetime on the sliding interface (Aubry et al., 2020; Dieterich & Kilgore, 1994; Rice, 2006). Based on an analogy with state evolution distance in RSF models, asperity sizes proposed in Rice (2006) are of the order of 5 μm, while slip localization thickness in well-established gouge is postulated in the same study to be in the range 10–20 μm, and up to 100–300 μm in natural principal slip zone. Recent laboratory earthquakes experiments showed that the newly created gouge layer thickness is in the order of 10 μm, while post-mortem temperature estimates by carbon deposition techniques point toward asperity sizes of the order of 100 μm (Aubry et al., 2018, 2020).

In the case of granular and soft materials, temperature heterogeneities between grains (enhanced by extremely localized heat creation at particle contacts but attenuated by heat diffusion) seems to lead to melting in the areas where the strain rate is the largest. This partial melting would first concern the grains with the highest temperatures and the lowest melting points, but would not immediately lead to a large reduction in friction. Conversely, when the melt fraction increases, friction drop is moderate and the strain rate in the molten zone increases (Figure 13). In that specific case, the onset of melting does not act as a self-limiting phenomenon as often proposed, but would appear to have a positive feedback (Figure 11, right-hand panel). Under the assumptions of the present study, we can thus expect fault weakening to be more sudden than expected in most models. This process eventually stops when partial melting reaches values corresponding to a much larger fault weakening. Depending on normal stress and sliding velocity, a balance may be reached between heat creation and heat diffusion when the deformation is entirely localized.

In contrast with some theoretical models (Platt et al., 2014; Rice et al., 2014), our model does not invoke rate-dependent gouge dilatancy or rate-strengthening friction in order to prevent localization. When completely established, strain localization might be a self-limiting phenomenon because of a progressive shift from granular (prone to localization) to viscous (prone to de-localization) friction as the melt fraction increases in the interface.

5.3. Further Developments and Requirements for a Dynamic Friction Model

The numerical framework presented in the present study presents a large potential for future improvements. This includes the possibility to account in a more specific way for the mineralogy of the gouge (through grain morphologies, size distributions, and friction coefficients, for example), or to simulate grain comminution explicitly. It nevertheless has several limitations: (i) the reported simulations rely on a simple assumption in terms of melt distribution in the gouge layer (i.e., homogeneous distribution in a certain central layer of the gouge), (ii) the numerical model can only deal with heat creation and diffusion in an indirect way (relying on a second pass on stored results with back-calibrated contact thermal conductivities), and does not account for the dependency of melt viscosity on temperature, (iii) it only deals with steady-state simulations since it does not simulate the melting process explicitly (it can consider the initial presence of melt in a simulation, but not the change of phase), (iv) it leads to very long simulations which prevent extensive numerical campaigns, and (v) it is extremely local and cannot be strongly coupled with the overall dynamics of the seismic sliding of a whole fault.

A (semi-)analytical model seems necessary to go beyond these limitations. This model will have to take advantage of the results gathered in the numerical tests described in the present paper, in order to predict the friction coefficient and the shear rate profile at any time, based only on the distribution of the melt fraction in the interface. It will also have to deal with heat production and diffusion (between grains and in the surrounding medium), with melting enthalpy, with the dependence of the fluid viscosity with temperature, with the variations in space and time of the sliding velocity along the fault, and with the reduction of the thermal conductivity of the sheared gouge.

An important point will be the necessity to account for the mineral composition of the pulverized rock composing the gouge, since each grain made of a different mineral is expected to have a different melting point (Aubry et al., 2018). Finally, it will be necessary to connect it with the inertial effects in the surrounding medium. Eventually, we can expect the implementation of a temporal dimension in a more general semi-analytical model implemented at each discrete point of a fault surface. Another issue regarding comparisons with experiments is the model ability to predict the transient fault strengthening which is sometimes observed in high-velocity shear experiments before the establishment of a pervasive layer of molten rock (Hirose & Shimamoto, 2005). This strengthening is attributed to viscous resistance of the very first patches of melt, submitted to very large strain rates, before their merging and heating reduces both shear rate and viscosity and eventually leads to fault weakening.

6. Conclusion

Two sets of numerical simulations were undertaken in order to investigate shear-heating-related phenomena at the scale of granular fault gouge. The first one investigated the influence of the fault thickness during the first stages of the seismic sliding (i.e., before the first appearance of melt), while the second focused on the influence of the proportion of molten grains in the central area of a gouge layer. We found that granular gouges naturally tend to localize shearing in a narrow area, corresponding to a few tens of the average grain diameter. Instantaneous strain rate profiles were even found to be thinner (e.g., about ten grains diameters), but switching rapidly from one active site to another during sliding. The temperature distribution in a given layer of the gouge was nearly Gaussian, with standard deviations of a few Kelvins. It was observed that, upon shearing, the bulk thermal conductivity of the gouge was divided by a factor 2.5, because of the dilatancy-induced loss of a large number of mechanical contacts.

The introduction of molten grains in the central area of the fault gouge led to a reduction in friction. This friction reduction is not proportional to the amount of melt, but nonlinear, following a sigmoid-like weakening as a function of melt proportion. The respective contributions of the solid and molten grains in the resistance to shear showed that solid grains resist less to shearing than what would be expected from a linear mixing law, because melt lubricates their contacts. In contrast, molten grains resist more than expected because they experience larger local strain rates when trapped between solid grains. Melt presence leads to a more intense localization of the shearing, and thus to fast fault weakening. This positive feedback stops when the amount of melt gives to the interface a sufficiently viscous character. The requirements for a fu-

ture friction law accounting for all these phenomena were listed, in the perspective of introducing such a law in semi-analytical dynamic simulations of seismic sliding.

Data Availability Statement

All simulations were performed with the open-source software MELODY version 3.94 (https://doi.org/10.5281/zenodo.4305614) developed by the first author and described in Mollon (2018). Simulation data can be found at: Mollon, Guilhem (2020), "Simulating melting in seismic fault gouge", Mendeley Data, V1, https://doi.org/10.17632/n8bwrtzsjd.1.

Acknowledgments
The authors acknowledge that this study contains original material, as a result of a purely academic study without any kind of private funding or conflict of interest. Its publication has been approved tacitly by the responsible authorities at the institutes where the work has been carried out.

References

Anthony, J. L., & Marone, C. (2005). Influence of particle characteristics on granular friction. *Journal of Geophysical Research*, *110*, B08409. https://doi.org/10.1029/2004jb003399

Arzi, A. A. (1978). Critical phenomena in the rheology of partially melted rocks. *Tectonophysics*, *44*, 173–184. https://doi.org/10.1016/0040-1951(78)90069-0

Aubry, J., Passelègue, F. X., Deldicque, D., Girault, F., Marty, S., Lahfid, A., et al. (2018). Frictional heating processes and energy budget during laboratory earthquakes. *Geophysical Research Letters*, *45*(12), 274–282. https://doi.org/10.1029/2018gl079263

Aubry, J., Passelègue, F. X., Escartin, J., Gasc, J., Deldicque, D., & Schubnel, A. (2020). Fault stability across the seismogenic zone. *Journal of Geophysical Research: Solid Earth*, *125*(8), e2020JB019670. https://doi.org/10.1029/2020jb019670

Bizzarri, A. (2009). Can flash heating of asperity contacts prevent melting? *Geophysical Research Letters*, *36*, L11304. https://doi.org/10.1029/2009gl037335

Cardwell, R. K., Chinn, D. S., Moore, G. F., & Turcotte, D. L. (1978). Frictional heating on a fault zone with finite thickness. *Geophysical Journal International*, *52*, 525–530. https://doi.org/10.1111/j.1365-246x.1978.tb04247.x

Costa, A., Caricchi, L., & Bagdassarov, N. (2009). A model for the rheology of particle-bearing suspensions and partially molten rocks. *Geochemistry, Geophysics, Geosystems*, *10*(3), Q03010. https://doi.org/10.1029/2008gc002138

Coussot, P., & Ancey, C. (1999). Rheophysical classification of concentrated suspensions and granular pastes. *Physical Review E: Statistical Physics, Plasmas, Fluids, and Related Interdisciplinary Topics*, *59*, 4445–4457. https://doi.org/10.1103/physreve.59.4445

Cundall, P. A., & Strack, O. D. L. (1979). A discrete numerical model for granular assemblies. *Géotechnique*, *29*, 47–65. https://doi.org/10.1680/geot.1979.29.1.47

Dieterich, J. H., & Kilgore, B. D. (1994). Direct observationof frictional contacts: New insights for state-dependent properties. *Pure and Applied Geophysics*, *143*(1–3), 283–302. https://doi.org/10.1007/bf00874332

Di Toro, G., Goldsby, D. L., & Tullis, T. E. (2004). Friction falls toward zero in quartz rock as slip velocity approaches seismic rates. *Nature*, *427*(6973), 436–439. https://doi.org/10.1038/nature02249

Di Toro, G., Hirose, T., Nielsen, S., Pennacchioni, G., & Shimamoto, T. (2006). Natural and experimental evidence of melt lubrication of faults during earthquakes. *Science*, *311*(1), 647–649. https://doi.org/10.1126/science.1121012

Forterre, Y., & Pouliquen, O. (2008). Flows of dense granular media. *Annual Review of Fluid Mechanics*, *40*, 1–24. https://doi.org/10.1146/annurev.fluid.40.111406.102142

Frank, F. C. (1965). On Dilatancy in Relation to Seismic Sources. *Reviews of Geophysics*, *3*(4), 485–503. https://doi.org/10.1029/rg003i004p00485

Frye, K. M., & Marone, C. (2002). The effect of particle dimensionality on granular friction in laboratory shear zones. *Geophysical Research Letters*, *29*(19), 1916. https://doi.org/10.1029/2002gl015709

Goldsby, D. L., & Tullis, T. E. (2002). Low frictional strength of quartz rocks at subseismic slip rate. *Geophysical Research Letters*, *29*(17), 1844. https://doi.org/10.1029/2002gl015240

Goldsby, D. L., & Tullis, T. E. (2011). Flash heating leads to low frictional strength of crustal rocks at earthquake slip rates. *Science*, *334*(6053), 216–218. https://doi.org/10.1126/science.1207902

Guo, N., & Zhao, J. (2016). 3D multiscale modeling of strain localization in granular media. *Computers and Geotechnics*, *80*, 360–372. https://doi.org/10.1016/j.compgeo.2016.01.020

Guo, Y., & Morgan, J. K. (2007). Fault gouge evolution and its dependence on normal stress and rock strength – Results of discrete element simulations: Gouge zone properties. *Journal of Geophysical Research*, *112*, B10403. https://doi.org/10.1029/2006jb004524

Hall, S. A., Muir Wood, D., Ibraim, E., & Viggiani, G. (2010). Localised deformation patterning in 2D granular materials revealed by digital image correlation. *Granular Matter*, *12*, 1–14. https://doi.org/10.1007/s10035-009-0155-1

Han, R., Hirose, T., & Shimamoto, T. (2010). Strong velocity weakening and powder lubrication of simulated carbonate faults at seismic slip rates. *Journal of Geophysical Research*, *115*(3), B03412. https://doi.org/10.1029/2008jb006136

Han, R., Shimamoto, T., Hirose, T., Ree, J. H., & Ando, J. (2007). Ultralow friction of carbonate faults caused by thermal decomposition. *Science*, *316*, 7–12. https://doi.org/10.1126/science.1139763

Hirose, T., & Shimamoto, T. (2005). Growth of molten zone as a mechanism of slip weakening of simulated faults in gabbro during frictional melting. *Journal of Geophysical Research*, *110*(5), 1–18. https://doi.org/10.1029/2004jb003207

Iordanoff, I., Fillot, N., & Berthier, Y. (2005). Numerical study of a thin layer of cohesive particles under plane shearing. *Powder Technology*, *159*, 46–54. https://doi.org/10.1016/j.powtec.2005.05.053

Kono, Y., Kenney-Benson, C., Hummer, D., Ohfuji, H., Park, C., Shen, G., et al. (2014). Ultralow viscosity of carbonate melts at high pressures. *Nature Communications*, *5*, 5091. https://doi.org/10.1038/ncomms6091

Lockner, D., Moore, D., Beeler, N., & Kilgore, B. (2010), *Surface melt produced on faults during laboratory stick-slip experiments*. Abstract T23A-2245 presented at 2010 Fall Meeting, San Francisco, CA: AGU.

Ma, X., & Elbanna, A. (2018). Strain localization in dry sheared granular materials: A compactivity-based approach. *Physical Review*, *98*, 022906. https://doi.org/10.1103/physreve.98.022906

Madhusudana, C. V., & Ling, F. F. (1995). *Thermal contact conductance* (p. 184). Springer.

Mair, K., Frye, K. M., & Marone, C. (2002). Influence of grains characteristics on the friction of granular shear zones. *Journal of Geophysical Research*, *107*(B10), 2219. https://doi.org/10.1029/2001jb000516
Mair, K., & Marone, C. (2000). Shear heating in granular layers. *Pure and Applied Geophysics*, *157*, 1847–1866. https://doi.org/10.1007/pl00001064
Mead, W. J. (1925). The geologic role of dilatancy. *The Journal of Geology*, *33*(7). https://doi.org/10.1086/623241
MiDi. (2004). On dense granular flows. *The European Physical Journal E*, *14*, 341–365.
Mollon, G. (2015). A numerical framework for discrete modelling of friction and wear using Voronoi polyhedrons. *Tribology International*, *90*, 343–355. https://doi.org/10.1016/j.triboint.2015.04.011
Mollon, G. (2018). A unified numerical framework for rigid and compliant granular materials. *Computational Particle Mechanics*, *5*, 517–527. https://doi.org/10.1007/s40571-018-0187-6
Mollon, G. (2019). Solid flow regimes in dry sliding contacts. *Tribology Letters*, *67*, 120. https://doi.org/10.1007/s11249-019-1233-0
Mollon, G., Quacquarelli, A., Andò, E., & Viggiani, G. (2020). Can friction replace roughness in the numerical simulation of granular materials? *Granular Matter*, *22*, 42. https://doi.org/10.1007/s10035-020-1004-5
Mollon, G., & Zhao, J. (2012). Fourier-Voronoi-based generation of realistic samples for discrete modelling of granular materials. *Granular Matter*, *14*, 621–638. https://doi.org/10.1007/s10035-012-0356-x
Muto, J., Nakatani, T., Nishikawa, O., & Nagahama, H. (2015). Fractal particle size distribution of pulverized fault rocks as a function of distance from the fault core. *Geophysical Research Letters*, *42*, 3811–3819. https://doi.org/10.1002/2015gl064026
Nielsen, S., Di Toro, G., Hirose, T., & Shimamoto, T. (2008). Frictional melt and seismic slip. *Journal of Geophysical Research*, *113*(1), 1–20. https://doi.org/10.1029/2007jb005122
Passelègue, F. X., Schubnel, A., Nielsen, S., Bhat, H. S., Deldicque, D., & Madariaga, R. (2016). Dynamic rupture processes inferred from laboratory microearthquakes. *Journal of Geophysical Research: Solid Earth*, *121*, 4343–4365. https://doi.org/10.1002/2015jb012694
Platt, J. D., Rudnicki, J. W., & Rice, J. R. (2014). Stability and localization of rapid shear in fluid-saturated fault gouge: 2. Localized zone width and strength evolution. *Journal of Geophysical Research: Solid Earth*, *119*, 4334–4359. https://doi.org/10.1002/2013jb010711
Pozzi, G., De Paola, N., Holdsworth, R. E., Bowen, L., Nielsen, S. B., & Dempsey, E. D. (2019). Coseismic ultramylonites: An investigation of nanoscale viscous flow and fault weakening during seismic slip. *Earth and Planetary Science Letters*, *516*, 164–175. https://doi.org/10.1016/j.epsl.2019.03.042
Reches, Z. e., & Lockner, D. A. (2010). Fault weakening and earthquake instability by powder lubrication. *Nature*, *467*(7314), 452–455. https://doi.org/10.1038/nature09348
Renouf, M., Cao, H.-P., & Nhu, V.-H. (2011). Multiphysical modeling of third-body rheology. *Tribology International*, *44*, 417–425. https://doi.org/10.1016/j.triboint.2010.11.017
Reynolds, O. (1901). *Scientific Papers*, *II*.
Rice, J. R. (2006). Heating and weakening of faults during earthquake slip. *Journal of Geophysical Research*, *111*(5), 1–29. https://doi.org/10.1029/2005jb004006
Rice, J. R., Rudnicki, J. W., & Platt, J. D. (2014). Stability and localization of rapid shear in fluid-saturated fault gouge: 1. Linearized stability analysis. *Journal of Geophysical Research: Solid Earth*, *119*, 4311–4333. https://doi.org/10.1002/2013jb010710
Salerno, K. M., Bolintineanu, D. S., Grest, G. S., Lechmann, J. B., Plimpton, S. J., Srivastava, I., & Silbert, L. E. (2018). Effect of shape and friction on the packing and flow of granular materials. *Physical Review*, *98*, 050901. https://doi.org/10.1103/physreve.98.050901
Sone, H., & Shimamoto, T. (2009). Frictional resistance of fault during accelerating and decelerating earthquake slip. *Nature Geoscience*, *2*, 750–708. https://doi.org/10.1038/ngeo637
Sulem, J., Famin, V., & Noda, H. (2009). Thermal decomposition of carbonates in fault zones: Slip-weakening and temperature-limiting effects. *Journal of Geophysical Research*, *114*(B6), 1–14. https://doi.org/10.1029/2009jb006576
Tian, J., Liu, E., & He, C. (2020). Shear band analysis of granular materials considering effects of particle shape. *Acta Mechanica*, *231*, 4445–4461. https://doi.org/10.1007/s00707-020-02771-y
Torsedillas, A., Peters, J. F., & Gardiner, B. S. (2004). Shear band evolution and accumulated microstructural development in Cosserat media. *International Journal for Numerical and Analytical Methods in Geomechanics*, *28*, 981–1010.
Vosteen, H.-D., & Schellschmidt, R. (2003). Influence of temperature on thermal conductivity, thermal capacity and thermal diffusivity for different types of rock. *Physics and Chemistry of the Earth*, *28*, 499–509. https://doi.org/10.1016/s1474-7065(03)00069-x
Wang, R., Cao, W., & Zhang, J.-M. (2019). Dependency of dilatancy ratio on fabric anisotropy in granular materials. *Journal of Engineering Mechanics*, *145*(10), 04019076. https://doi.org/10.1061/(asce)em.1943-7889.0001660
Wibberley, C. A. J., & Shimamoto, T. (2005). Earthquake slip weakening and asperities explained by thermal pressurization. *Nature*, *436*(7051), 689–692. https://doi.org/10.1038/nature03901
Yao, L., Ma, S., Platt, J. D., Niemeijer, A. R., & Shimamoto, T. (2016). The crucial role of temperature in high-velocity weakening of faults: Experiments on gouge using host blocks with different thermal conductivities. *Geology*, *44*(1), 63–66. https://doi.org/10.1130/g37310.1
Zhao, S., Evans, T. M., & Zhou, X. (2018). Shear-Induced anisotropy of granular materials with rolling resistance and particle shape effects. *International Journal of Solids and Structures*, *150*, 268–281. https://doi.org/10.1016/j.ijsolstr.2018.06.024